J. Mech. Phys. Solids Vol. 41, No. 1, pp. 183–211, 1993.
Printed in Great Britain.

0022–5096/93 $5.00+0.00

COMPRESSIVE FAILURE OF FIBRE COMPOSITES

B. BUDIANSKY

Division of Applied Sciences, Harvard University, Cambridge, MA 02138, U.S.A.

and

N. A. FLECK

Cambridge University Engineering Department, Trumpington Street, Cambridge, CB2 1PZ, U.K.

(*Received* 2 *December* 1991)

ABSTRACT

A REVIEW OF experimental data and elementary theoretical formulas for compressive failure of polymer matrix fibre composites indicates that the dominant failure mode is by plastic kinking. Initial local fibre misalignment plays a central role in the plastic kinking process. Theoretical analyses and numerical results for compressive kinking are presented, encompassing effects of strain-hardening, kink inclination, and applied shear stress. The assumption of rigid fibres is assessed critically, and the legitimacy of its use for polymer matrix composites is established.

INTRODUCTION

COMPRESSION FAILURE is a design limiting feature of aligned, continuous fibre composite materials. For example, the compressive strengths of unidirectional carbon fibre–epoxy laminates are often less than 60% of their tensile strengths. The dominant compressive failure mode in aligned-fibre, polymeric matrix composites is localized compressive buckling, or kinking; other failure modes, such as fibre crushing, can also occur. Although fibre kinking limits the compressive strength of carbon-matrix composites, and has often been observed in wood, the importance of kinking in metal-matrix and ceramic-matrix composites generally is not yet clear.

The present paper, continuing the recent studies of FLECK and BUDIANSKY (1991), is concerned primarily with various aspects of the compressive kinking problem. A preliminary discussion invokes theoretical arguments and existing experimental information to support the belief that the kinking mechanism in polymer-matrix and carbon-matrix fibre composites is dominated by fibre misalignment together with plastic shear deformation in the matrix. This sets the stage for the extension of previous theoretical results for static kinking strength under combined compression and shear to include effects of composite strain-hardening.

As in most treatments of compressive kinking the fibres in these calculations are

assumed to be rigid with respect to longitudinal straining. This has the effect of shielding the matrix from axial stress, and therefore the actual effect of this stress on matrix plasticity is not taken into account. The present paper concludes with calculations of the influence on kinking stress of finite fibre stiffness, and parameter ranges are revealed for which the rigid-fibre assumption is acceptable.

The paper deals only with the response of unidirectional un-notched composites. In many practical applications notched multi-directional composites are used. Engineering design methodologies are now emerging to deal with the effects of notches and off-axis plies (e.g. STARNES and WILLIAMS, 1982; RHODES *et al.*, 1984; SOUTIS *et al.*, 1990) but basic mechanics modelling of these more complex systems remains to be done.

COMPRESSIVE FAILURE MODES: BACKGROUND AND REVIEW

Elastic kinking vs plastic kinking

Microbuckling under axial compression of aligned-fibre composities is a failure mechanism wherein (see Fig. 1) the fibres undergo cooperative kinking in a narrow band. Observations show typical values of band width w in the neighbourhood of 10 fibre diameters, and values in the range $\beta \approx 10°$–$30°$ for the inclination of the kink band. On the basis of the assumptions that the kinking is an *elastic* bifurcation-buckling phenomenon, and that $\beta = 0$, ROSEN (1965) derived the widely-quoted formula

$$\sigma_c = \frac{G_m}{1 - v_f} \tag{1}$$

for the kinking stress, where G_m is the shear modulus of the matrix material, and v_f is the volumetric fraction of fibres. The Rosen result should actually be interpreted as $\sigma_c = G$, where G is the effective longitudinal shear modulus of the *composite*, and the

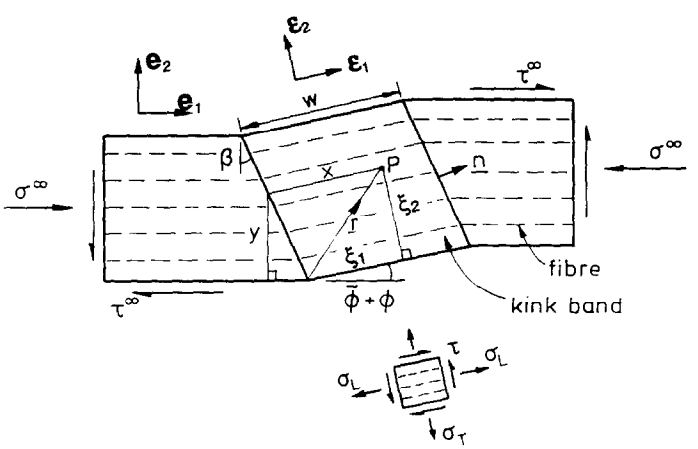

FIG. 1. Kink band geometry and notation.

right-hand side of (1) is just an approximation for G. ARGON (1972) took the alternative view that long-fibre composites undergo *plastic* microbuckling. He assumed, in effect, that kinking occurs in a $\beta = 0$ band within which fibres have suffered an initial misalignment angle $\bar{\phi}$ (see Fig. 1). In a rigid-perfectly plastic composite having yield stress τ_Y in longitudinal shear, additional rotation ϕ cannot develop until the critical compressive stress

$$\sigma_c = \frac{\tau_Y}{\bar{\phi}} \tag{2}$$

is applied, and subsequently the compressive stress decreases with increasing ϕ.

The Argon formula (2) for the plastic kinking stress was extended by BUDIANSKY (1983) to an *elastic*-perfectly plastic composite, with yield strain $\gamma_Y = \tau_Y/G$ in longitudinal shear, for which the kinking stress is

$$\sigma_c = \frac{\tau_Y}{\gamma_Y + \bar{\phi}} = \frac{G}{1 + \bar{\phi}/\gamma_Y}. \tag{3}$$

This result (still for $\beta = 0$) is uniformly valid for all $\bar{\phi}$, giving the Rosen bifurcation stress for $\bar{\phi} = 0$, and asymptotically equivalent to the Argon result (2) for $\bar{\phi}$ large.

JELF and FLECK (1991) measured the microbuckling stresses of linear elastic composites made from glass fibres and a silicone rubber matrix. They observed microbuckles having half-wavelengths equal to the specimen length, and found that as the specimen length was increased the compressive strength decreased towards the Rosen limit (1). However, available experimental evidence for more conventional polymer matrix composites supports the hypothesis that microbuckling is a plastic rather than an elastic event. Test data from a variety of sources for the axial compressive strength σ_c of aligned-fibre polymer matrix composites are plotted against G in Fig. 2. [The

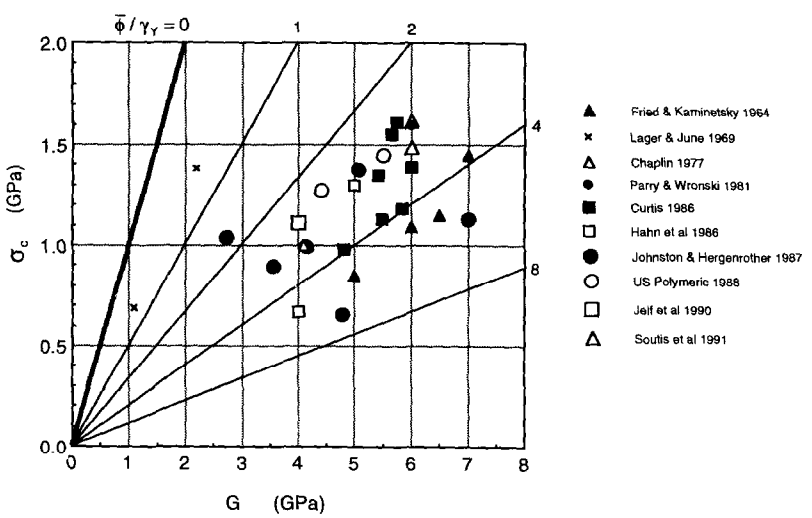

FIG. 2. Test data and elastic-ideally plastic predictions, compressive strength σ_c vs composite shear modulus G, for zero-inclination kink bands ($\beta = 0°$). Fibre misalignment = $\bar{\phi}$, shear yield strain = γ_Y.

composite G values were estimated via the right-hand side of (1), and, in turn, each G_m was calculated from estimates, measurements or handbook values of the Young's modulus E_m and Poisson's ratio ν_m of the matrix.] The elastic kinking stress is given by the heavy line (corresponding to $\bar{\phi}/\gamma_Y = 0$) and the other slanted straight lines are plots of (3) for several values of $\bar{\phi}/\gamma_Y > 0$. The simplifying assumptions (e.g., $\beta = 0$, ideal plasticity) used in the derivation of (3) limit its direct applicability; indeed, more realistic analyses, taking into account strain-hardening as well as $\beta > 0$ will be made in this paper. We note, nevertheless, that most of the data in Fig. 2 fall well below the elastic buckling line, and are consistent with (3) for a range of values of $\bar{\phi}/\gamma_Y$ near 4. If we set γ_Y equal to some nominal magnitude—say 1%—this gives values of $\bar{\phi}$ scattered about a mean value in the vicinity of 2°. As we shall see later, this rough estimate for typical values of $\bar{\phi}$ may change somewhat in the light of more refined calculations, but it is in good agreement with measured values of the misalignment of fibre bundles when a laminate was sectioned and examined under a light microscope by YURGARTIS (1987). Yurgartis found that most of the fibres in a carbon fibre-PEEK unidirectional composite were oriented within ±3° of the mean fibre direction, and the standard deviation of the distribution was 1.9°.

Indirect evidence to support (3) comes from compression tests on woven carbon fibre cloth by WILKINSON *et al.* (1986). They found that the compressive strength of T300/914 carbon–epoxy cloth ($G \approx 6$ GPa) decreased from about 1 GPa to 200 MPa when they inserted brass wires into the cloth normal to the fibre direction in order to increase the waviness. From these strength measurements the inferred value of $\bar{\phi}/\gamma_Y$ increases from 5 to 29 via (3). With $\gamma_Y \approx 0.01$ (0.57°) this corresponds to an increase of $\bar{\phi}$ from 3° to 17°. These theoretical values agree well with our measurements of the maximum fibre bundle waviness from the micrographs published by WILKINSON *et al.* (1986), which show increases from approximately 3° to approximately 20°.

The compressive strength of composites shows a large degree of scatter, with nominally identical specimens often varying in strength by 25%. This is consistent with plastic microbuckling, for which the analytic prediction (3) shows high imperfection sensitivity, with strength strongly dependent upon the misalignment angle. In contrast, the *elastic* microbuckling collapse load is fairly insensitive to imperfections (BUDIANSKY, 1979), and would not show much scatter.

The simple formula (3) for the kinking stress of an elastic-ideally plastic composite under pure longitudinal compression, kinking in a band normal to the fibre direction, provides an indication of the relative importance of the physical parameters that govern the kinking strength. It follows from (3) that variations $\delta\tau_Y$, δG and $\delta\bar{\phi}$ in the shear yield stress, elastic shear modulus, and initial misalignment are related to a change $\delta\sigma_c$ in the kinking stress by

$$\frac{\delta\sigma_c}{\sigma_c} = \left(\frac{\sigma_c}{G}\right)\frac{\delta G}{G} + \left(1 - \frac{\sigma_c}{G}\right)\frac{\delta\tau_Y}{\tau_Y} - \left(1 - \frac{\sigma_c}{G}\right)\frac{\delta\bar{\phi}}{\bar{\phi}}. \tag{4}$$

Thus, to give a typical example, if $\sigma_c/G = 1/4$, a fractional increase of yield stress is three times as effective in raising the kinking stress as is a similar relative change in the shear modulus, and the same is true for a fractional decrease in the initial imperfection.

Plastic kinking vs fibre crushing

In an illuminating set of tests (PIGGOT and HARRIS, 1980; PIGGOTT, 1981), the modulus of a polyester resin matrix was varied by partial curing, and it was found that the matrix yield strength varied proportionally. With reinforcing fibres of either glass or Kevlar, and $v_f = 0.31$, a nominal, uniform value of $\gamma_Y \approx 0.024$ (1.4°) for the composites can be estimated from their data. Figure 3 shows the measured composite strengths on another plot of σ_c versus G. Again we infer a value $\bar{\phi} \approx 2°$ for both the glass and Kevlar fibres from the initial, nearly linear ranges of the data, presumed to reflect plastic kinking. However, above transitional values of the composite stiffness G, the failure-stress levels, shown by the arrows in Fig. 3, become more-or-less independent of G (or of $\tau_Y = G\gamma_Y$). Piggot and Harris surmise that in this range failure was due to *fibre crushing*.

Fibre failure in compression crushing occurs when the uniaxial strain in the composite equals the intrinsic crushing strain ε_{fc} of the fibres. A variety of mechanisms may be associated with fibre crushing. In the case of steel fibres local crushing is due to plastic yielding (MONCUNILL DE FERRAN and HARRIS, 1970; PIGGOTT and WILDE, 1980). Glass fibres tend to fail in compression by longitudinal splitting. In the case of carbon, Kevlar and wood fibres, local buckling or kinking occurs *within* each fibre (GRESZCZUK, 1972, 1975; PRANDY and HAHN, 1990; YOUNG and YOUNG, 1990; PIGGOTT and HARRIS, 1980; GIBSON and ASHBY, 1988); kink bands within the fibres of width less than the fiber radius are observed (PRANDY and HAHN, 1990). Pitch-based carbon fibres have a very well aligned longitudinal microstructure, and they fail in compression by a combination of internal buckling and longitudinal splitting. Typical values of crushing strain are $\varepsilon_{fc} = 0.5\%$ for Kevlar and pitch-based carbon fibres, and $\varepsilon_{fc} = 2.5\%$ for PAN-based carbon fibres.

The average axial stress in the composite at which fibre crushing occurs is given

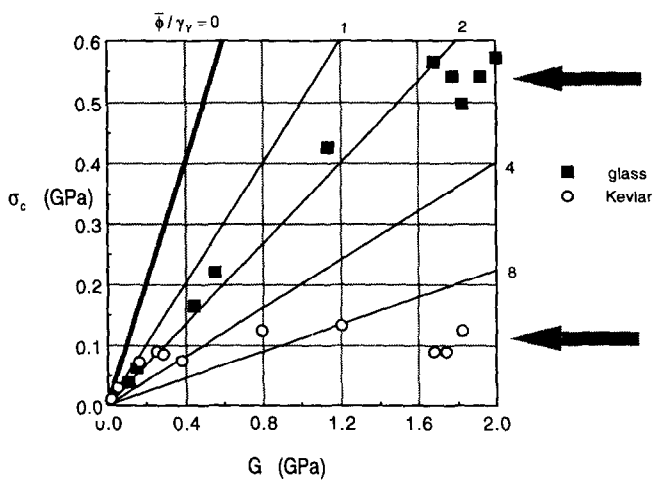

FIG. 3. Test data (PIGGOTT and HARRIS, 1980; PIGGOTT, 1981) for compressive strengths of glass and Kevlar fibre reinforced, partially cured resins. Arrows indicate presumed stress levels at transitions from kinking to fibre crushing.

approximately by the rule-of-mixtures formula $\sigma_c = [v_f E_f + (1 - v_f)E_m]\varepsilon_{fc}$, where E_f is the Young's modulus of the fibres. In the Piggott–Harris tests, $E_m/E_f \ll 1$, and so the fibre crushing strengths $\sigma_{fc} = E_f \varepsilon_{fc}$ can be estimated as $\sigma_{fc} \approx \sigma_c/v_f$ from the upper-shelf values of σ_c. This gives fibre crushing strengths of about 1.7 and 0.4 GPa for the glass and Kevlar, respectively; these values are plausible.

Early carbon fibre–epoxy matrix systems were manufactured from carbon fibres of low crushing strength and epoxies of high yield strength. These materials failed by fibre crushing at test temperatures below approximately 100°C (EWINS and POTTER, 1980). At higher temperatures the yield strength of the early epoxies drops sufficiently for the failure mechanism to switch to kinking. More modern carbon fibre–epoxy systems possess carbon fibres of higher crushing strength, and a tougher, lower yield strength matrix. The transition temperature from fibre crushing to kinking is shifted from 100°C to −40°C, and modern carbon fibre–epoxy laminates fail by kinking at both ambient and elevated temperatures (BARKER and BALASUNDARAM, 1987).

Shear banding

Finally, we remark that besides fibre crushing and localized kinking, another distinct failure mode has been observed in aligned-fibre polymer-matrix composites with very low fibre volume fractions, namely *shear-banding*, oriented at about 45° with respect to the loading axis (FRIED, 1963). This is a failure mode essentially identical to that which would occur in the unreinforced matrix material, to which the few fibres present offer little resistance, and is not expected to be significant at conventional fibre volume fractions.

Carbon, ceramic and metal matrices

Microbuckling in carbon–carbon composites has been observed by EVANS and ADLER (1978) and CHATTERJEE and MCLAUGHLIN (1979). The latter found compressive strengths as low as 1/20 of the elastic kinking stress (1), and suggested plastic kinking as the operative failure mechanism. The plasticity of the carbon matrix is probably due primarily to microcracking. Similar nonlinear stress–strain behaviour due to matrix microcracking and consequent kinking mechanisms might also be expected in some ceramic–matrix composites. Although little experimental evidence is available, LANKFORD (1989) did observe kinking at high compressive strain rates in a pyroceramic matrix reinforced with silicon carbide fibres. His measured compressive strength of $\sigma_c \approx 1500$ MPa, and our roughly estimated values of $\tau_Y \approx 115$ MPa and $\gamma_Y \approx 0.01$, when substituted into the plastic kinking formula (3), give $\bar{\phi} \approx 4°$ for the fibre misalignment.

Compressive failure in metal-matrix fibre composites has received little study, and the importance of kinking as a failure mode in such composites has not been established.

MATRIX STRAIN-HARDENING EFFECTS ON KINKING

We shall now analyse the kinking of an aligned-fibre composite, taking into account the influence of plastic strain-hardening in the matrix. Combined compression and

shear loading of the composite will be considered, as will arbitrary kink-band orientations. As in previous studies (e.g., FLECK and BUDIANSKY, 1991), fibre inextensibility will be assumed, and fibre bending resistance will be neglected. A critical assessment of the assumptions of fibre inextensibility will be made later in this paper. The significance of fibre bending will be addressed in a future publication.

We presume that in the presence of remotely applied compressive and shear stresses σ^∞ and τ^∞, there exists a kinked band (see Fig. 1) of infinite extent and finite width w, currently oriented at an angle β. With $\sigma^\infty = \tau^\infty = 0$, the band is imagined to have an initial orientation angle β_0, and is given an initial imperfection characterized by a uniform fibre rotation $\bar{\phi}$. We smear out the material to obtain an anisotropic continuum in a state of plane strain. Neglecting the fibre bending stiffness implies that the continuum is free of couple stresses, and that, in effect, the fibres are broken at the two boundaries of the kink band. The deformation state is considered to be homogeneous but different inside and outside of the band. By asserting the continuity of tractions and displacements on the boundary of the band, and making use of the equations of equilibrium, kinematics and assumed constitutive relations for the anisotropic solid, the additional rotation ϕ inside the band, and its relation to the externally applied compressive and shear stresses σ^∞ and τ^∞, may be deduced.

Kinking equilibrium

As shown in Fig. 1, we let $(\mathbf{e}_1, \mathbf{e}_2)$ and $(\boldsymbol{\varepsilon}_1, \boldsymbol{\varepsilon}_2)$ be unit vectors parallel and perpendicular to the fibres outside and inside the kink band, respectively. Equating the tractions on each side of the band boundary gives

$$\mathbf{n}\cdot\boldsymbol{\sigma}^\infty = \mathbf{n}\cdot\boldsymbol{\sigma}, \tag{5}$$

where $\mathbf{n} = \mathbf{e}_1 \cos\beta + \mathbf{e}_2 \sin\beta$ is the unit normal to the band, the remote stress tensor $\boldsymbol{\sigma}^\infty$ is

$$\boldsymbol{\sigma}^\infty = -\sigma^\infty \mathbf{e}_1\mathbf{e}_1 + \tau^\infty(\mathbf{e}_1\mathbf{e}_2 + \mathbf{e}_2\mathbf{e}_1) \tag{6}$$

and the stress tensor $\boldsymbol{\sigma}$ inside the band is

$$\boldsymbol{\sigma} = \sigma_L \boldsymbol{\varepsilon}_1\boldsymbol{\varepsilon}_1 + \sigma_T \boldsymbol{\varepsilon}_2\boldsymbol{\varepsilon}_2 + \tau(\boldsymbol{\varepsilon}_1\boldsymbol{\varepsilon}_2 + \boldsymbol{\varepsilon}_2\boldsymbol{\varepsilon}_1). \tag{7}$$

Substitution of (6) and (7) into (5), and use of the connections

$$\mathbf{e}_1 = \boldsymbol{\varepsilon}_1 \cos(\phi + \bar{\phi}) - \boldsymbol{\varepsilon}_2 \sin(\phi + \bar{\phi}), \tag{8a}$$

$$\mathbf{e}_2 = \boldsymbol{\varepsilon}_1 \sin(\phi + \bar{\phi}) - \boldsymbol{\varepsilon}_2 \cos(\phi + \bar{\phi}), \tag{8b}$$

gives the two equilibrium statements

$$-\sigma^\infty \cos\beta \cos(\bar{\phi} + \phi) + \tau^\infty \sin(\beta + \bar{\phi} + \phi) = \tau \sin(\beta - \bar{\phi} - \phi) + \sigma_L \cos(\beta - \bar{\phi} - \phi), \tag{9}$$

$$\sigma^\infty \cos\beta \sin(\bar{\phi} + \phi) + \tau^\infty \cos(\beta + \bar{\phi} + \phi) = \tau \cos(\beta - \bar{\phi} - \phi) + \sigma_T \sin(\beta - \bar{\phi} - \phi). \tag{10}$$

The longitudinal stress σ_L along the fibre direction in the band is of limited interest (because the fibres are inextensible) and we need consider (9) no further. The stress

components and σ_T and τ will appear in the constitutive relations of the composite material, and (10) will play a central role in the calculation of the kinking response.

We assume henceforth that the initial imperfection $\bar{\phi}$ is small, and we anticipate that consideration of only small additional rotations ϕ will suffice to determine kinking strengths. Accordingly, it is appropriate to linearize (10) with respect to ϕ and $\bar{\phi}$. The linearized equation can be written in the form

$$(\phi+\bar{\phi})(\sigma^\infty \cos\beta - 2\tau^\infty \sin\beta) = [\tau-\tau^\infty][\cos\beta+(\phi+\bar{\phi})\sin\beta] + \sigma_T[\sin\beta-(\phi+\bar{\phi})\cos\beta]. \quad (11)$$

We can simplify further, dropping the terms containing $(\phi+\bar{\phi})$ in each of the square brackets on the right-hand side of (11) to get

$$\sigma^\infty - 2\tau^\infty \tan\beta = \frac{\tau-\tau^\infty+\sigma_T\tan\beta}{\phi+\bar{\phi}} \quad (12)$$

as the connection between the applied stresses $(\sigma^\infty, \tau^\infty)$, the rotation ϕ, and the stresses τ and σ_T that develop in the kinked band.

(We note, incidentally, that the time derivatives $\dot{\sigma}_T$ and $\dot{\tau}$ of the stresses defined, as shown in Fig. 1, with respect to the rotating fibre directions are objective stress rates which are *not* equal to the Jaumann stress rates. Nevertheless, they appear to be the natural choices to appear in constitutive relations that involve stress rates.)

Kinking kinematics

In both the kinked and unkinked regions, inextensibility implies zero strain in the fibre direction. Outside of the kink band we stipulate zero rotation, and zero direct strain transverse to the fibre direction. Accordingly, to within rigid body motion, the velocity $\mathbf{v}$ in the unkinked region to the left of the kink (Fig. 1) is simply

$$\mathbf{v} = y\dot{\gamma}^\infty \mathbf{e}_1, \quad (13)$$

where $\dot{\gamma}^\infty$ is the remote shear strain rate parallel to the fibres. Inside the kink band the velocity of a point P is

$$\mathbf{v} = y\dot{\gamma}^\infty \mathbf{e}_1 + x\dot{\phi}\boldsymbol{\varepsilon}_2. \quad (14)$$

The strain rate tensor in the band is

$$\dot{\boldsymbol{\varepsilon}} = \tfrac{1}{2}[\nabla\mathbf{v}+(\nabla\mathbf{v})^T], \quad (15)$$

where the superscript T denotes the transpose, and the gradient operator ∇ is

$$\nabla = \boldsymbol{\varepsilon}_1 \frac{\partial}{\partial\xi_1} + \boldsymbol{\varepsilon}_2 \frac{\partial}{\partial\xi_2}. \quad (16)$$

The position $\mathbf{r}$ of point P is

$$\mathbf{r} = \xi_1\boldsymbol{\varepsilon}_1 + \xi_2\boldsymbol{\varepsilon}_2 = y(-\mathbf{e}_1\tan\beta+\mathbf{e}_2)+x\boldsymbol{\varepsilon}_1. \quad (17)$$

The unit-vector connections (8) then give

$$\left.\begin{aligned} x &= \xi_1 + \xi_2 \tan(\beta - \phi - \bar{\phi}) \\ y &= \xi_2 \cos\beta \sec(\beta - \phi - \bar{\phi}) \end{aligned}\right\} \tag{18}$$

and the velocity (14), rewritten in terms of $(\xi_1, \dot{\xi}_1, \varepsilon_1, \varepsilon_2)$, may be used in (15) to give the strain velocity tensor

$$\begin{aligned} \dot{\boldsymbol{\varepsilon}} = {} & \tfrac{1}{2}[\boldsymbol{\varepsilon}_1\boldsymbol{\varepsilon}_2 + \boldsymbol{\varepsilon}_2\boldsymbol{\varepsilon}_1][\dot{\phi} + \dot{\gamma}^{\infty} \cos\beta \sec(\beta - \phi - \bar{\phi}) \cos(\phi + \bar{\phi})] \\ & + \boldsymbol{\varepsilon}_2\boldsymbol{\varepsilon}_2[\dot{\phi} \tan(\beta - \phi - \bar{\phi}) - \dot{\gamma}^{\infty} \cos\beta \sec(\beta - \phi - \bar{\phi}) \sin(\phi + \bar{\phi})] \end{aligned} \tag{19}$$

in the kink band. However, $\dot{\boldsymbol{\varepsilon}} \equiv \frac{1}{2}\dot{\gamma}[\boldsymbol{\varepsilon}_1\boldsymbol{\varepsilon}_2 + \boldsymbol{\varepsilon}_2\boldsymbol{\varepsilon}_1] + \dot{e}_T\boldsymbol{\varepsilon}_2\boldsymbol{\varepsilon}_2$, where by definition $\dot{\gamma}$ is the shear strain rate in the band and $\dot{e}_T$ is the direct strain rate transverse to the fibres. Identification of this expression for $\dot{\boldsymbol{\varepsilon}}$ with (19) gives

$$\dot{\gamma} = \dot{\phi} + \dot{\gamma}^{\infty} \cos\beta \sec(\beta - \phi - \bar{\phi}) \cos(\phi + \bar{\phi}) \tag{20a}$$

and

$$\dot{e}_T = \dot{\phi} \tan(\beta - \phi - \bar{\phi}) - \dot{\gamma}^{\infty} \cos\beta \sec(\beta - \phi - \bar{\phi}) \sin(\phi + \bar{\phi}). \tag{20b}$$

From (17), $\dot{\mathbf{r}} = (-y\dot{\beta}\sec^2\beta)\mathbf{e}_1 + x\dot{\varepsilon}_1 \equiv \mathbf{v}$, and with $\dot{\varepsilon}_1 = \dot{\phi}\varepsilon_2$, it follows from (14) that

$$\dot{\beta} = -\dot{\gamma}^{\infty} \cos^2\beta. \tag{21}$$

This integrates to

$$\tan\beta = \tan\beta^0 - \gamma^{\infty}, \tag{22}$$

where β^0 corresponds to the kink angle associated with vanishing remote shear strain.

For $\gamma^{\infty} \equiv 0$, $\beta = \beta^0$ and (20a, b) may be integrated to give

$$\gamma = \phi \tag{23a}$$

and

$$e_T = \log\left[\frac{\cos(\beta - \phi - \bar{\phi})}{\cos(\beta - \bar{\phi})}\right]. \tag{23b}$$

For small values of γ^{∞}, ϕ and $\bar{\phi}$, we can ignore the difference between β and β^0, linearize (20a, b), and integrate to get

$$\gamma = \phi + \gamma^{\infty}, \tag{24a}$$

$$e_T = \phi \tan\beta. \tag{24b}$$

We remark here that a non-zero e_T, together with the assumptions of inextensibility and plane strain, implies that the kinked material undergoes volumetric straining. The early stages of plastic deformation in polymers (and also carbon matrices) may indeed be associated with volume changes attributable to the opening of microcracks and voids (PURSLOW, 1986). This is consistent with the observation that the von Mises effective stress for flow in polymers increases with an increase of pressure (WARD, 1983).

Constitutive relations

The combined-stress yield condition

$$\left(\frac{\tau}{\tau_Y}\right)^2 + \left(\frac{\sigma_T}{\sigma_{TY}}\right)^2 = 1 \tag{25}$$

has been used by BUDIANSKY (1983) and FLECK and BUDIANSKY (1991) for the ideally-plastic, inextensible composite. Here τ_Y and σ_{TY} are the plane-strain yield stresses in pure shear and pure transverse tension. This may be generalized to the strain-hardening case by defining

$$\tau_e = \sqrt{\tau^2 + \sigma_T^2/R^2} \tag{26}$$

as an effective stress that must increase during plastic straining, and using $\tau_e(\tau, \sigma_T)$ as a plastic potential for the plastic strain rates $\dot{\gamma}^p$ and $\dot{e}_T^p$. Note that $\tau_e(\tau, \sigma_T)$ is a homogeneous function of degree one, that the current yield ellipse in (τ, σ_T) space expands homogeneously with increasing τ_e, and that the constant parameter R, defining the eccentricity of the yield ellipse, is the ratio σ_{TY}/τ_Y of the yield stresses in transverse tension and shear.

For monotonically increasing τ_e, the flow-theory relations connecting plastic strain rates with the plastic potential may be postulated as

$$\dot{\gamma}^p = F(\tau_e)\frac{\partial \tau_e}{\partial \tau}\dot{\tau}_e,$$

$$\dot{e}_T^p = F(\tau_e)\frac{\partial \tau_e}{\partial \sigma_T}\dot{\tau}_e. \tag{27}$$

Let $\dot{\gamma}_e^p$ be a *work-equivalent* effective strain rate (HILL, 1979) defined by

$$\tau\dot{\gamma}^p + \sigma_T\dot{e}_T^p = \tau_e\dot{\gamma}_e^p. \tag{28}$$

It follows that

$$\dot{\gamma}_e^p = F(\tau_e)\dot{\tau}_e \tag{29}$$

and that (27) are equivalent to

$$\mathrm{d}\gamma^p = \frac{\partial \tau_e}{\partial \tau}\mathrm{d}\gamma_e^p,$$

$$\mathrm{d}e_T^p = \frac{\partial \tau_e}{\partial \sigma_T}\mathrm{d}\gamma_e^p, \tag{30}$$

where γ_e^p is an effective plastic strain that depends only on τ_e. Further, the relationship between γ_e^p and τ_e must be the same as that between γ^p and τ in pure shear.

For proportional loading, during which τ and σ_T maintains a constant ratio, the partial derivatives in (30) remain constant, and integration gives

$$\gamma^p = \frac{\partial \tau_e}{\partial \tau}\gamma_e^p,$$

$$e_T^p = \frac{\partial \tau_e}{\partial \sigma_T} \gamma_e^p. \tag{31}$$

These relations have the form of a loading-path-independent *deformation theory* of plasticity, that we shall use in the rest of this paper, even if proportional loading conditions are not quite met. (Briefly, the justification for pursuing the easier calculations afforded by deformation theory is as follows: in the kinking problem, the kink stresses, at least up to maximum load, do stay approximately proportional, and deformation theory, reinterpreted as a *corner* theory of plasticity, is then physically acceptable (BUDIANSKY, 1959); and in plastic buckling problems, deformation theories are well-known to give better answers than flow theories.)

We can rewrite (31) as

$$\gamma^p = \left(\frac{\gamma_e^p}{\tau_e}\right)\tau = \left(\frac{1}{G_s(\tau_e)} - \frac{1}{G}\right)\tau,$$

$$e_T^p = \left(\frac{\gamma_e^p}{\tau_e}\right)\frac{\sigma_T}{R^2} = \left(\frac{1}{G_s(\tau_e)} - \frac{1}{G}\right)\frac{\sigma_T}{R^2}, \tag{32}$$

where the function $G_s(\tau)$ is the pure-shear secant modulus. The total strains, elastic plus plastic, are then

$$\gamma = \frac{\tau}{G} + \left(\frac{\gamma_e^p}{\tau_e}\right)\tau = \frac{\tau}{G_s(\tau_e)} \tag{33}$$

and

$$e_T = \frac{\sigma_T}{E_T} + \left(\frac{\gamma_e^p}{\tau_e}\right)\frac{\sigma_T}{R^2} = \frac{\sigma_T}{E_T} + \left(\frac{1}{G_s(\tau_e)} - \frac{1}{G}\right)\frac{\sigma_T}{R^2}, \tag{34}$$

where E_T is an effective transverse Young's modulus. (It is appreciated that imposition of the condition of plane strain on the *total* strains in the kink band would really couple the constitutive rules for the elastic and plastic components of strain, but the simple decoupled formulation should suffice for the purpose of the present exploratory studies.) We now make a final simplification of these constitutive relations, by arbitrarily setting

$$\frac{E_T}{G} = R^2 = \left(\frac{\sigma_{TY}}{\tau_Y}\right)^2 \tag{35}$$

and this lets us write

$$\gamma = \frac{\tau}{G_s(\tau_e)},$$

$$e_T = \frac{\sigma_T}{R^2 G_s(\tau_e)}. \tag{36}$$

We note also that if we define

$$\gamma_e \equiv \frac{\tau_e}{G_s(\tau_e)}, \tag{37}$$

we have

$$\gamma_e = \sqrt{\gamma^2 + R^2 e_T^2} \tag{38}$$

and (36) can be rewritten as

$$\gamma = \left(\frac{\gamma_e}{\tau_e}\right)\tau,$$

$$e_T = \left(\frac{\gamma_e}{\tau_e}\right)\frac{\sigma_T}{R^2}. \tag{39}$$

To implement the constitutive relations explicitly, we shall adopt the three-parameter (G, τ_Y, n) Ramberg–Osgood representation

$$\gamma = \frac{\tau}{G}\left[1 + \frac{3}{7}\left(\frac{\tau}{\tau_Y}\right)^{n-1}\right] \tag{40}$$

for the shear stress–strain curve of the composite. Here, for strain-hardening, τ_Y is defined as a nominal composite yield stress for which the secant modulus $G_s(\tau) = \tau/\gamma$ of the composite is reduced to 70% of its initial elastic value G. For $n = \infty$, (40) gives the elastic-ideally plastic stress–strain relation; $\tau_Y = \infty$ provides elastic behaviour. If we define

$$\gamma_Y \equiv \frac{\tau_Y}{G} \tag{41}$$

as the elastic strain of the composite at $\tau = \tau_Y$, we can write the non-dimensional relations

$$\frac{\gamma}{\gamma_Y} = \frac{\tau}{\tau_Y} + \frac{3}{7}\left(\frac{\tau}{\tau_Y}\right)^n \tag{42}$$

and

$$\frac{G}{G_s(\tau)} = 1 + \frac{3}{7}\left(\frac{\tau}{\tau_Y}\right)^{n-1}. \tag{43}$$

Under combined stressing (40), (42) and (43) remain valid with τ and γ replaced by τ_e and γ_e.

Kinking analysis and results for pure compression loading; experimental data

We consider first the case of zero kink angle β, for which $e_T = 0$ for small rotation ϕ. For a given initial rotation $\bar{\phi}$ (assumed positive here and henceforth) and a pure compressive loading stress σ^∞, the equilibrium equation (12) gives

$$\sigma^{\infty} = \frac{\tau}{\phi + \bar{\phi}} \tag{44}$$

in the kink band. With $\phi = \gamma$ from (23a), we get

$$\frac{\sigma^{\infty}}{G} = \frac{\tau/\tau_Y}{\gamma/\gamma_Y + \bar{\phi}/\gamma_Y} \tag{45}$$

and with the use of the Ramberg Osgood relation (42) this is found to be a maximum with respect to τ/τ_Y, and hence ϕ, at

$$\tau/\tau_Y = \left[\frac{7(\bar{\phi}/\gamma_Y)}{3(n-1)}\right]^{1/n} \tag{46}$$

and

$$\phi/\gamma_Y = \gamma/\gamma_Y = \left[\frac{7(\bar{\phi}/\gamma_Y)}{3(n-1)}\right]^{1/n} + \frac{\bar{\phi}/\gamma_Y}{n-1}. \tag{47}$$

The corresponding maximum value of (45) provides the kinking stress σ_c given by

$$\frac{\sigma_c}{G} = \frac{1}{1 + n\left(\frac{3}{7}\right)^{1/n}\left(\frac{\bar{\phi}/\gamma_Y}{n-1}\right)^{(n-1)/n}}. \tag{48}$$

For $n = \infty$, this reduces to the elastic-perfectly plastic result of (4).

Equation (48) may be regarded as a knockdown factor that must be applied to the elastic (Rosen) kinking stress due to plasticity and initial imperfections. Figure 4 shows how σ_c/G varies with $\bar{\phi}/\gamma_Y$ for $n = 3$, 5, 9 and ∞. Note that strain-hardening does not change the elastic-perfectly plastic value of σ_c very much.

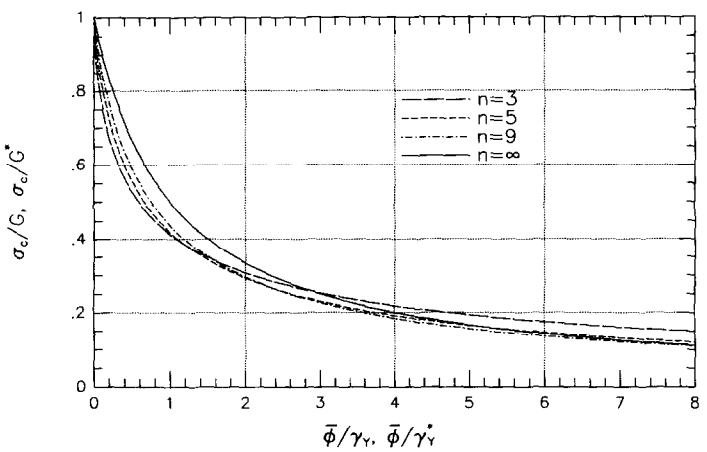

FIG. 4. Non-dimensional kinking stress ratio σ_c/G vs imperfection ratio $\bar{\phi}/\gamma_Y$ ($\beta = 0$), or σ_c/G^* vs $\bar{\phi}/\gamma_Y^*$ ($\beta > 0$), for various values of the Ramberg–Osgood hardening parameter n. ($G^* = \alpha^2 G$, $\gamma_Y^* = \gamma_Y/\alpha$, $\alpha^2 = 1 + R^2 \tan^2 \beta$, $R = \sigma_{TY}/\tau_Y$.)

For a given imperfection size $\bar{\phi}/\gamma_Y$ we can minimize (48) with respect to n in order to determine the largest possible effect of strain-hardening plasticity on the kinking stress. The resulting minimum value of σ_c/G is

$$\left(\frac{\sigma_c}{G}\right)_{\min} = \left(\tfrac{10}{7} + \bar{\phi}/\gamma_Y\right)^{-1} \tag{49}$$

for the value

$$n = 1 + \tfrac{7}{3}(\bar{\phi}/\gamma_Y) \tag{50}$$

of the strain-hardening index.

For a given $\bar{\phi}/\gamma_Y$, the result (49) and the largest prediction of (48) for n in the range $(3, \infty)$ prescribe plausible theoretical bounds for σ_c. These bounds are compared in Fig. 5 with the experimental data of Fig. 2, as well as with the portion of the Piggott–Harris data for kinking of Fig. 3. The lower boundary of each shaded band represents the minimum σ_c given by (49); the top boundary is given by $n = \infty$ for $\bar{\phi}/\gamma_Y = 1$ and 2, and by $n = 3$ for $\bar{\phi}/\gamma_Y = 4$ and 8. The conclusion we draw from this comparison is that the inferred predominant values of $\bar{\phi}/\gamma_Y \approx 4$ are hardly changed from the earlier estimate made on the basis of $n = \infty$. However all of this, of course, is still for an assumed kink angle $\beta = 0$.

We can now easily modify the analysis to cover $\beta > 0$. Equation (12) becomes (with τ^∞ still zero)

$$\sigma^\infty = \frac{\tau + \sigma_T \tan\beta}{\phi + \bar{\phi}}. \tag{51}$$

With $\gamma^\infty = 0$, and ϕ positive, (24), (38)–(39) imply

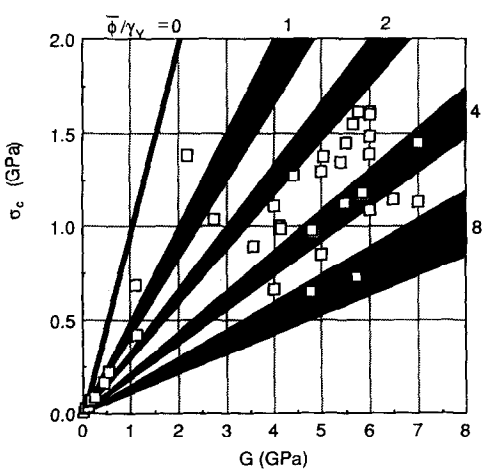

FIG. 5. Test data and elastic strain-hardening predictions for $\beta = 0$; the shaded region for each $\bar{\phi}/\gamma_Y$ shows the range of the theoretical results for n in $(3, \infty)$.

$$\tau + \sigma_T \tan\beta = \tau_e \sqrt{1 + R^2 \tan^2 \beta} \tag{52}$$

and

$$\gamma_e = \phi \sqrt{1 + R^2 \tan^2 \beta}. \tag{53}$$

If we introduce the definitions

$$\alpha \equiv \sqrt{1 + R^2 \tan^2 \beta}, \tag{54}$$

$$\gamma_Y^* \equiv \gamma_Y / \alpha, \tag{55}$$

$$G^* \equiv \alpha^2 G, \tag{56}$$

then (51) implies

$$\frac{\sigma^\infty}{G^*} = \frac{\tau_e / \tau_Y}{\gamma_e / \gamma_Y + \bar{\phi} / \gamma_Y^*}. \tag{57}$$

Comparing this with (45), and remembering that (42) holds with τ and γ replaced by τ_c and γ_c, shows that the earlier result for the kinking stress given by (48) continues to apply with G and γ_Y replaced by G^* and γ_Y^*. Hence,

$$\frac{\sigma_c}{G^*} = \frac{1}{1 + n(\frac{3}{7})^{1/n} \left(\dfrac{\bar{\phi}/\gamma_Y^*}{n-1} \right)^{(n-1)/n}}, \tag{58}$$

which provides the curves previously plotted in Fig. 4.

To see how the comparison with experimental data is modified for a typical kink angle, it is convenient to rewrite (58) in the form

$$\frac{\sigma_c}{G} = \frac{1 + R^2 \tan^2 \beta}{1 + n(\frac{3}{7})^{1/n} \left[\dfrac{\bar{\phi}/\gamma_Y}{n-1} \sqrt{1 + R^2 \tan^2 \beta} \right]^{(n-1)/n}}. \tag{59}$$

For a given value of $\bar{\phi}/\gamma_Y$ this has the minimum value

$$\left(\frac{\sigma_c}{G} \right)_{\min} = [1 + R^2 \tan^2 \beta][\tfrac{10}{7} + (\bar{\phi}/\gamma_Y) \sqrt{1 + R^2 \tan^2 \beta}]^{-1} \tag{60}$$

for

$$n = 1 + \tfrac{7}{3}(\bar{\phi}/\gamma_Y) \sqrt{1 + R^2 \tan^2 \beta}. \tag{61}$$

Once again, we show the experimental data for σ_c vs G in Fig. 6, but the theoretical bands for each $\bar{\phi}/\gamma_Y$ are now based on (60)–(61) for n in (3, ∞), with $\beta = 20^\circ$ and $R^2 = E_T/G = (\sigma_{TY}/\tau_Y)^2 = 4$. (The heavy solid line has been kept at the elastic prediction for $\beta = 0$.) The inferred characteristic average values of $\bar{\phi}/\gamma_Y \approx 5$, and hence $\bar{\phi} \approx 3^\circ$, are now somewhat larger than those estimated on the basis of $\beta = 0$.

The present analysis does not predict observed kink angles; for any given n and $\bar{\phi}/\gamma_Y$ the lowest value of σ_c predicted by (59) always corresponds to $\beta = 0$. A separate study (BUDIANSKY, 1983) suggests that the non-uniform waviness induced by com-

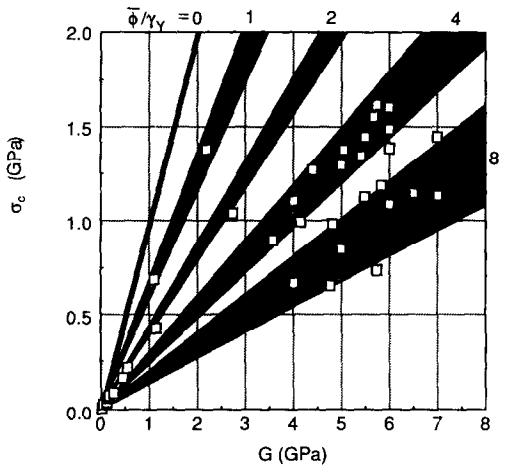

FIG. 6. Test data and strain-hardening predictions for $\beta = 20^\circ$ and $E_T/G = (\sigma_{TY}/\tau_Y)^2 = 4$; the shaded region for each $\bar{\phi}/\gamma_Y$ shows the range of the theoretical results for n in $(3, \infty)$.

pressive load acting on localized fibre misalignments tends to organize itself into skewed patterns that lock the kinking into inclined bands.

The Ramberg–Osgood stress–strain equation has facilitated numerical studies of strain-hardening effects, but its use is not, of course, essential. [Some early plastic kinking calculations by CHATTERJEE and MCLAUGHLIN (1979) for $\beta = 0$ were, in fact, based on (44), and the use of a bilinear τ–γ relation.] We conclude this section by showing, for an *arbitrary* τ_e–γ_e relation, a simple graphical interpretation of the maximization of σ^*, as given by (51), to get σ_c. [The same kind of construction has been described by BATDORF and KO (1987) and others for similar equations; the idea may be traced back to Considère in the last century, in connection with the ultimate tensile strength of ductile bars.] It is convenient to work with (57) for σ^*/G^*, with γ_Y now defined arbitrarily, but γ_Y^* and G^* still given by (55)–(56). Figure 7 shows the normalized stress–strain curve of τ_e/τ_Y vs γ_e/γ_Y. The point A has the coordinates $(-\bar{\phi}/\gamma_Y^*, 0)$, and so, by (57), as the point P moves up along the stress–strain curve,

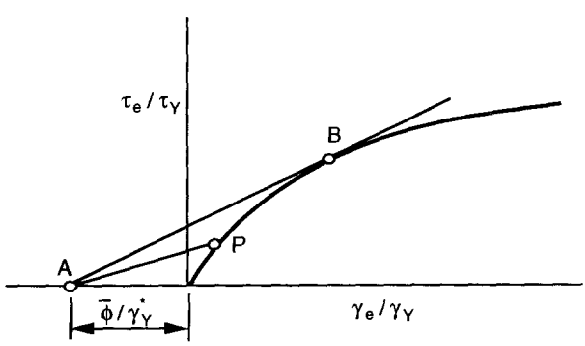

FIG. 7. Considère diagram; σ_c/G^* is equal to the slope of line AB.

the slope of the line AP is σ^∞/G^*. This slope is a maximum, and therefore equal to σ_c/G^*, when P reaches the point B where AB is tangent to the curve.

Kinking analysis and results, combined compression and shear

We shall assume that the remotely applied shear stress τ^∞ is fixed during the subsequent compressive loading (see Fig. 1), and consider first the case $\beta = 0$. Using $\phi = \gamma - \gamma^\infty$ (24a) in (12) gives

$$\sigma^\infty = \frac{\tau - \tau^\infty}{\gamma - \gamma^\infty + \bar{\phi}}. \tag{62}$$

(This differs slightly from the equation given by BATDORF and KO (1987), who appear to have been the first to consider the effect of applied shear stress on kinking; they omit the term γ^∞.) Non-dimensionalizing, we get

$$\frac{\sigma^\infty}{G} = \frac{\tau/\tau_Y - \tau^\infty/\tau_Y}{(\gamma/\gamma_Y - \gamma^\infty/\gamma_Y) + \bar{\phi}/\gamma_Y}. \tag{63}$$

Figure 8(a) shows how to modify the Considère diagram of Fig. 7 in order to represent (63). The slope of the tangent line AB still gives σ_c/G, but now the coordinates of the point A are at $(-\bar{\phi}/\gamma_Y + \gamma^\infty/\gamma_Y, \tau^\infty/\tau_Y)$. The modified Considère diagram for the case of an elastic-ideally plastic material ($n = \infty$) is shown in Fig. 8(b). Ideal plasticity requires that we keep $\tau^\infty < \tau_Y$. The slope of AB is $(1 - \tau^\infty/\tau_Y)/(1 - \gamma^\infty/\gamma_Y + \bar{\phi}/\gamma_Y)$, and so

$$\frac{\sigma_c}{G} = \left[1 + \left(\frac{\bar{\phi}/\gamma_Y}{1 - \tau^\infty/\tau_Y}\right)\right]^{-1} \tag{64}$$

for ideal plasticity. In this case, therefore, the effect of an applied shear stress is exactly equivalent to that of an increased initial fibre misalignment.

To compute σ_c in the case of strain-hardening, we write

$$t = \tau/\tau_Y, \quad \eta = \gamma/\gamma_Y, \quad t^\infty = \tau^\infty/\tau_Y, \quad \text{and} \quad \eta^\infty = \gamma^\infty/\gamma_Y \tag{65}$$

in (63) and set $\mathrm{d}(\sigma^\infty/G)/\mathrm{d}t = 0$ to get

$$\sigma_c/G = 1/\eta'(t),$$

$$\bar{\phi}/\gamma_Y = \frac{t - t^\infty}{\sigma_c/G} - \eta + \eta^\infty \tag{66}$$

as combinations of σ_c/G and $\bar{\phi}/\gamma_Y$ generated parametrically by values of $t > t^\infty$. This holds for smooth stress–strain curves, for which $\eta(t)$ is a continuously differentiable, monotonically increasing function of t, and $\eta'(t) \equiv \mathrm{d}\eta/\mathrm{d}t$.

For Ramberg–Osgood stress–strain relations, the formula for $\eta(t)$ given by (42) was used in (66) to generate the curves for $n = 3$ in Fig. 9(a), for $\tau^\infty/\tau_Y = 0$, 0.5 and 0.8. The corresponding curves for $n = \infty$, based on (65), are shown in Fig. 9(b).

Turning next to the consideration of $\beta \neq 0$, we substitute the constitutive relations (39) and the strain–rotation formulas (24) in the equilibrium equation (12) to get

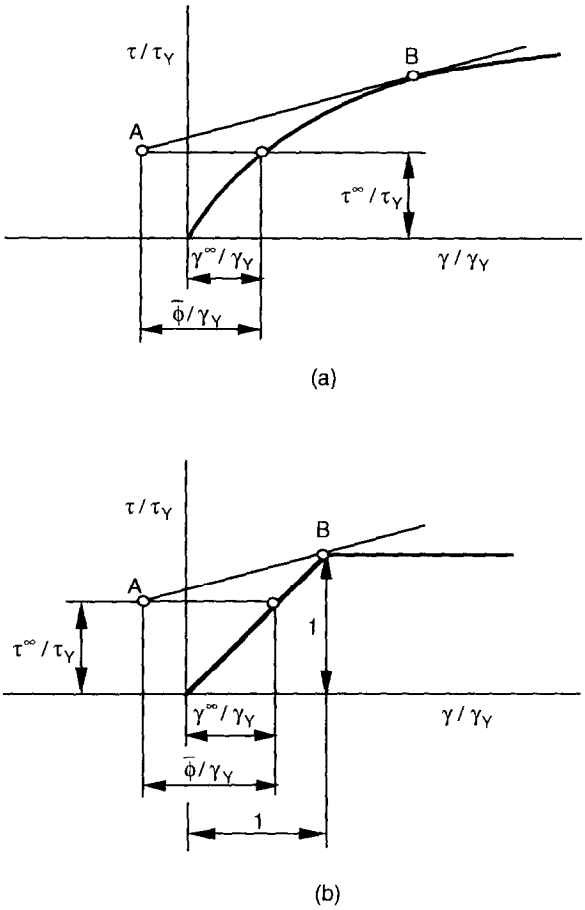

FIG. 8. Modified Considère diagrams for combined compression and shear, with $\beta = 0$. For both (a) strain-hardening and (b) ideal plasticity, σ_e/G is equal to the slope of line AB.

$$\sigma^{\infty} - 2\tau^{\infty} \tan\beta = \frac{[(1+R^2\tan^2\beta)\phi + \gamma^{\infty}]\tau_e - \tau^{\infty}\gamma_e}{(\phi+\bar{\phi})\gamma_e}, \tag{67a}$$

where

$$\gamma_e^2 = (1+R^2\tan^2\beta)\phi^2 + 2\phi\gamma^{\infty} + (\gamma^{\infty})^2. \tag{67b}$$

With the adjusted definitions $t = t_e/\tau_Y$, $\eta = \gamma_e/\gamma_Y$, the notational substitutions $\omega = \phi/\gamma_Y$, $\bar{\omega} = \bar{\phi}/\gamma_Y$, and the definition (54) for α, we find

$$A \equiv \frac{\sigma^{\infty} - 2\tau^{\infty}\tan\beta}{G} = \frac{(t/\eta)[\alpha^2\omega + \eta^{\infty}] - t^{\infty}}{\omega+\bar{\omega}}, \tag{68}$$

where

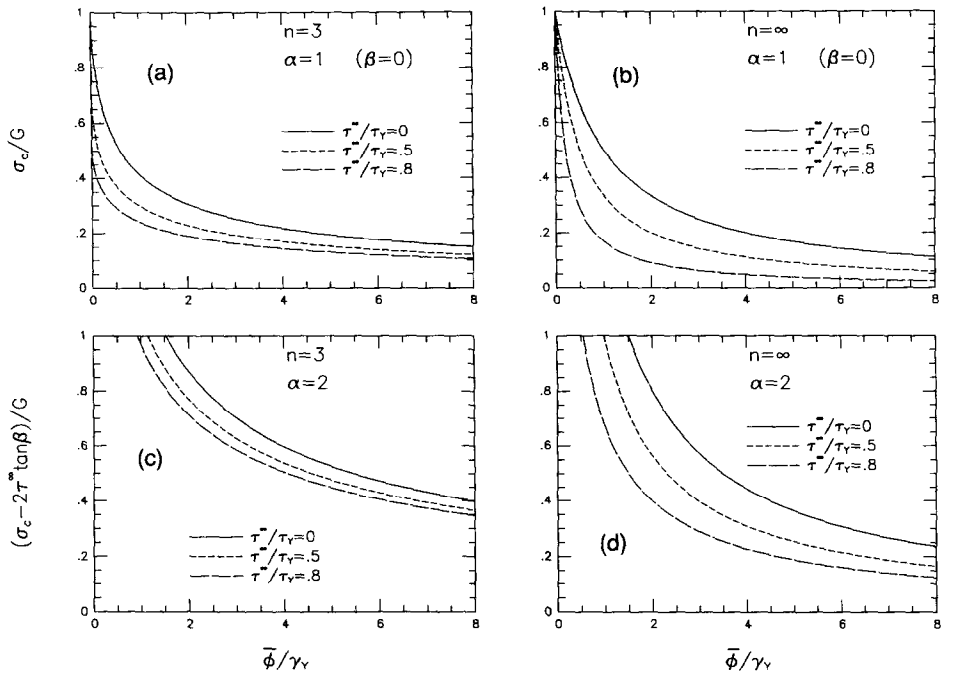

FIG. 9. Theoretical results for kinking under combined shear and compression; $\alpha^2 = 1 + R^2 \tan^2\beta$, $R = \sigma_{TY}/\tau_Y$.

$$\eta = \sqrt{\alpha^2\omega^2 + 2\omega\eta^\infty + (\eta^\infty)^2}. \tag{69}$$

Setting $dA/d\omega = 0$ leads to the parametric equations

$$A_c \equiv \frac{\sigma_c - 2\tau^\infty \tan\beta}{G} = \alpha^2 \frac{dt}{d\eta} + \left[\frac{t}{\eta} - \frac{dt}{d\eta}\right]\left[\frac{\eta^\infty}{\eta}\right]^2 [\alpha^2 - 1],$$

$$\bar{\omega} \equiv \frac{\bar{\phi}}{\gamma_Y} = \frac{(\tau/\eta)[\alpha^2\omega + \eta^\infty] - t^\infty}{A_c} - \omega \tag{70}$$

for A_c vs $\bar{\omega}$. An efficient procedure to generate the solution for a given value of t^∞ (and hence η^∞) is to assume values of ω, get η via (69), and find t and $dt/d\eta$ from the shear stress–strain relation, inverting it numerically, if necessary. Unfortunately, there does not appear to be a neat Considère diagram that goes with these results for $\beta > 0$. Furthermore, although we were able to parameterize α out of the results for $\tau^\infty = 0$ [see (58a, b)], this is not possible for $\tau^\infty > 0$. For this reason, it is no longer useful to show results for the kinking stress as a function of the modified imperfection parameter $\bar{\phi}/\gamma_Y^*$. Thus, Fig. 9(c) shows the numerical results produced by (70) for A_c vs $\bar{\omega} = \bar{\phi}/\gamma_Y$, for $n = 3$ and $\alpha = 2$.

For $n = \infty$, we must again assume $\tau^\infty/\tau_Y < 1$, as we did for $\beta = 0$, and in the expression (68) for A we can set $\eta^\infty = t^\infty$. For $\tau^\infty = 0$, the maximum value of A is attained at the onset of plasticity, but not necessarily for $\tau^\infty > 0$. For any given value

of τ^{∞}/τ_Y, there is a critical transition value $\bar{\omega}_T$ such that, for $\bar{\phi}/\gamma_Y < \bar{\omega}_T$, A_c is given by the yield condition $\eta = 1$ in (68). For higher values of $\bar{\phi}/\gamma_Y$, (70) (with $\mathrm{d}t/\mathrm{d}\eta = 0$) govern the relation between A_c and $\bar{\omega}$. In the examples shown in Fig. 9(d) for $n = \infty$, the transition values $\bar{\omega}_T$ were found to be 1.411 and 0.174, for $\tau^{\infty}/\tau_Y = 0.5$ and 0.8, respectively. For $\bar{\omega} > \bar{\omega}_T$ the stress state (τ, σ_T) moves around the yield locus (25) between the onset of yield and the attainment of the maximum applied stress σ_c, and so the loading is far from proportional. The applicability of a deformation theory therefore becomes questionable, but as in buckling problems generally, the results for σ_c are lower than those that would be given by a possibly more realistic flow theory, and are therefore conservative. However these reservations should not be taken too seriously, since the yield condition (25) is anyhow, arbitrary, imperfection magnitudes are uncertain, and the present results for $\beta \neq 0$ should be regarded as indicative of trends rather than precise predictions.

It should be noted that for $\tau^{\infty}/\tau_Y \leqslant 1$, the term containing τ^{∞} in the numerator of the expression in (70) for A_c is usually negligible compared to σ_c, because $\tau^{\infty}/G = \gamma_Y(\tau^{\infty}/\tau_Y)$ is small compared to A_c. So A_c is a good approximation to σ_c/G. Note, however, that σ_c will be slightly smaller for $\beta < 0$ than for $\beta > 0$.

Fairly straightforward solution techniques can be used on (68)–(70) to generate results for A_c vs τ^{∞}/τ_Y for assigned values of $\bar{\phi}/\gamma_Y$. This has been done to evaluate the *shear knockdown factor* T, defined as

$$T \equiv \frac{A_c}{(\sigma_c/G)_{\tau^{\infty}=0}} = \frac{\sigma_c - 2\tau^{\infty}\tan\beta}{\sigma_c|_{\tau^{\infty}=0}}. \tag{71}$$

Here, for a Ramberg–Osgood material, the denominator is simply specified by (48). The results for T vs τ^{∞}/τ_Y are shown in Fig. 10, for $\bar{\phi}/\gamma_Y = 2$, 4 and 8, for $\alpha = 1$, 2, and $n = 3$, 5 and ∞. Again, since we can usually neglect the second term in the numerator of (71), T represents the *extra* knockdown factor that should be applied to the result (48) for σ_c to account for the presence of applied shear stress, while (48) itself is the knockdown factor applied to the Rosen result to account for fibre imperfection. Note that for $\bar{\phi}/\gamma_Y \geqslant 2$, T does not vary much with the size of the fibre misalignment.

Effects of Finite Fibre Stiffness

In this part of the paper we shall study and assess the simplifying assumption made in the kinking analysis that the fibres are infinitely stiff in their longitudinal directions. The main effect of finite axial fibre stiffness is to let the matrix carry a portion of the applied compressive stress, which can then interact with matrix shear and transverse stress to raise the level of plasticity, and lower the resistance to kinking. We shall demonstrate that, at least as far as organic-matrix composites are concerned, the rigid-fibre simplifying assumption does not have much effect on the validity of our kinking-stress calculations.

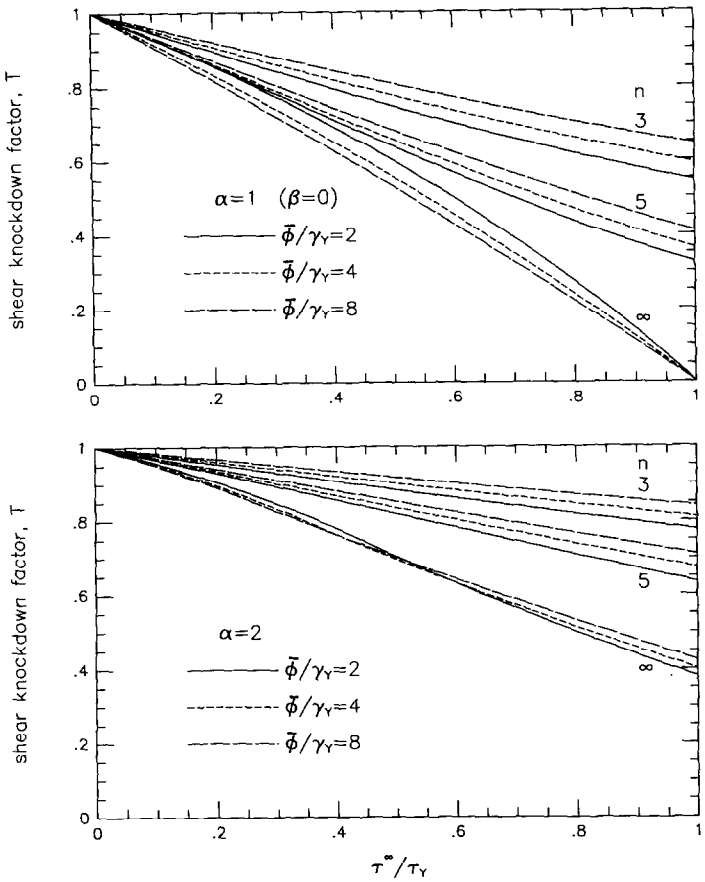

FIG. 10. Shear knockdown factor T vs τ^∞/τ_Y. For $\beta = 0$, T is the ratio of the compressive kinking stress when shear is present to the pure-compression kinking stress, and is close to this ratio for $\beta > 0$.

Perfectly aligned fibres

In a recent paper, ROSEN (1989) considered the influence of axial matrix compression on the microbuckling stress of composites having straight, perfectly aligned fibres, and for a Ramberg–Osgood value of $n = 3$, calculated a kinking stress on the basis of an effective, plasticity-reduced shear modulus used in place of the elastic shear modulus in his classical formula (1). In effect, Rosen used a deformation theory of plasticity to calculate this reduced modulus, and so shall we, but with a more accurate analysis of the pre-buckling stress state, and with more generality. We simplify matters greatly by limiting this study to $\beta = 0$, which lets us consider just combinations of shear τ_m and axial stress σ_m in the matrix.

Under the assumptions of initial isotropy and plastic incompressibility, *all* deformation theories of plasticity give the following result for the effective, initial shear modulus $\bar{G}_m$ of the matrix material when it is subjected to a purely uniaxial stress (PETERS *et al.*, 1950):

$$\bar{G}_m = \left[\frac{1}{G_m} + \frac{3}{E_{ms}(\sigma_m)} - \frac{3}{E_m}\right]^{-1}, \tag{72}$$

where, as indicated, the secant modulus E_{ms} of the matrix is a function of σ_m. It follows that the plastic bifurcation-buckling stress [see (1)] is now

$$\sigma_c = \frac{\bar{G}_m}{1-v_f} \tag{73}$$

and with $G \equiv G_m/(1-v_f)$,

$$\frac{\sigma_c}{G} = \left[1+\rho\left(\frac{E_m}{E_{ms}(\sigma_m)} - 1\right)\right]^{-1}, \tag{74}$$

where

$$\rho = 3G_m/E_m = 3/2(1+v_m). \tag{75}$$

Here E_{ms} depends on the value of σ_m when the critical stress σ_c is applied. These stresses, and the corresponding fibre stress σ_f, are connected by the very accurate rule-of-mixtures relation

$$\sigma_c = (1-v_f)\sigma_m + v_f\sigma_f \tag{76}$$

and the compatibility equation

$$\sigma_m/E_{ms}(\sigma_m) = \sigma_f/E_f, \tag{77}$$

where E_f is the modulus of the fibre, presumed to stay elastic. From these two relations we can derive another equation that relates σ_c and σ_m, to wit:

$$\frac{\sigma_c}{G} = \frac{\sigma_m(1-v_f)}{G_m}\left[1 - v_f + v_f\frac{E_f}{E_{ms}(\sigma_m)}\right]. \tag{78}$$

In principle, then, for any uniaxial relation between E_{ms} and σ_m, (74) and (78) can be solved simultaneously to get σ_c. It will be convenient, however, to show an explicit result for a Ramberg–Osgood family of matrix compression curves having the form

$$\frac{\varepsilon_m}{\varepsilon_{mY}} = \frac{\sigma_m}{\sigma_{mY}} + a\left(\frac{\sigma_m}{\sigma_{mY}}\right)^n. \tag{79}$$

Here σ_{mY} is a nominal matrix yield stress, $\varepsilon_{mY} \equiv \sigma_{mY}/E_m$, and a is a constant that, for the moment, we need not specify, except to note that $E_m/E_{ms} = (1+a)$ at $\sigma_m = \sigma_{mY}$. It follows that

$$\left(\frac{E_m}{E_{ms}} - 1\right) = a\left(\frac{\sigma_m}{\sigma_{mY}}\right)^{n-1} \tag{80}$$

and σ_m/σ_{mY} can be eliminated from (74) and (78) to give

$$\varepsilon_{mY} = \frac{\Lambda\left[\dfrac{\rho a\Lambda}{1-\Lambda}\right]^{1/(n-1)}}{2(1-v_f)(1+v_m)\left[1-v_f+\dfrac{v_f E_f}{E_m}\left(1+\dfrac{1-\Lambda}{\rho\Lambda}\right)\right]}, \tag{81}$$

where $\Lambda \equiv \sigma_c/G = \bar{G}_m/G_m$ is the *plasticity knockdown factor* for bifurcation buckling. This provides an explicit relation between the plasticity knockdown factor for the perfect-fibre composite and the nominal compressive yield strain of the matrix material.

We emphasize that this result is valid for *all* deformation theories of plasticity. We also mention, in passing, that all flow theories having smooth yield surfaces would predict *no* plasticity knockdown, because in such theories the initial shear modulus in the presence of an arbitrary axial stress remains equal to elastic value.

Before we show numerical examples, it will be useful to specialize to the familiar J_2-deformation theory in which the effective matrix stress for combined shear and compression is defined by

$$\sigma_{me} = \sqrt{\sigma_m^2 + 3\tau_m^2} \tag{82}$$

and the plastic strains are given by

$$\varepsilon_m^p = \left[\frac{E_m}{E_{ms}(\sigma_{me})} - 1\right]\frac{\sigma_m}{E_m}, \tag{83a}$$

$$\gamma_m^p = 3\left[\frac{E_m}{E_{ms}(\sigma_{me})} - 1\right]\frac{\tau_m}{E_m}. \tag{83b}$$

Here the bracketed quantities are given by (80) with σ_m replaced by σ_{me}. We can then touch base with our previous formulations in which the shear stress–strain curve of the *composite* was given by the Ramberg–Osgood form

$$\frac{\gamma}{\gamma_Y} = \frac{\tau}{\tau_Y} + b\left(\frac{\tau}{\tau_Y}\right)^n \tag{84}$$

with $b = 3/7$. As was implicit in the original Rosen equation (1), we make the rough approximations

$$\gamma = (1-v_f)\gamma_m, \quad \gamma_Y = (1-v_f)\gamma_{mY}, \quad \tau = \tau_m, \quad \tau_Y = \tau_{mY}, \tag{85}$$

appropriate for composites in which the longitudinal shear stiffness of the fibres is much greater than that of the matrix, to find that

$$\frac{\gamma_m}{\gamma_{mY}} = \frac{\tau_m}{\tau_{mY}} + b\left(\frac{\tau_m}{\tau_{mY}}\right)^n \tag{86}$$

is the shear stress–strain relation of the matrix. Then, since $\sigma_{me} = \tau_m\sqrt{3}$ for pure shear, comparison of (86) with (83b) shows that

$$\left[\frac{E_m}{E_{ms}} - 1\right] = \frac{b}{\rho}\left(\frac{\sigma_{me}}{\tau_{mY}\sqrt{3}}\right)^{n-1} \tag{87}$$

and if we introduce the definitions

$$\sigma_{mY} = \tau_{mY}\sqrt{3} \quad \text{and} \quad \varepsilon_{mY} = \sigma_{mY}/E_m, \tag{88}$$

we find from (83a) that for pure compression we recover (79), with $a = b/\rho$. Also, we have

$$\varepsilon_{mY} = \frac{\gamma_Y\sqrt{3}}{2(1+\nu_m)(1-v_f)} \tag{89}$$

and so (81) can be rewritten in the neat form

$$\gamma_Y = \frac{\Lambda\left[\frac{b\Lambda}{1-\Lambda}\right]^{1/(n-1)}}{\sqrt{3}\left[\frac{E}{E_m} + \left(\frac{E}{E_m} - 1 + v_f\right)\left(\frac{1-\Lambda}{\rho\Lambda}\right)\right]}, \tag{90}$$

where we have used the rule-of mixtures formula for the composite modulus $E = (1-v_f)E_m + v_f E_f$ in order to express the relation between Λ and γ_Y in terms of E/E_m instead of E_f/E_m.

Figure 11 shows the results given by (90) for $\Lambda \equiv \sigma_c/G$ vs γ_Y, for $n = 3$ and ∞, and for $E/E_m = 10$, 30 and 50. These values of E/E_m more than cover the practical range for organic-matrix composites, which usually have values in the interval 20–40. The curves were calculated for $v_f = 0.6$, but it should be noted that for large values of E/E_m, γ_Y is nearly independent of v_f. The other constants used were $\rho = 9/8$, corresponding to $\nu = 1/3$ and $b = 3/7$.

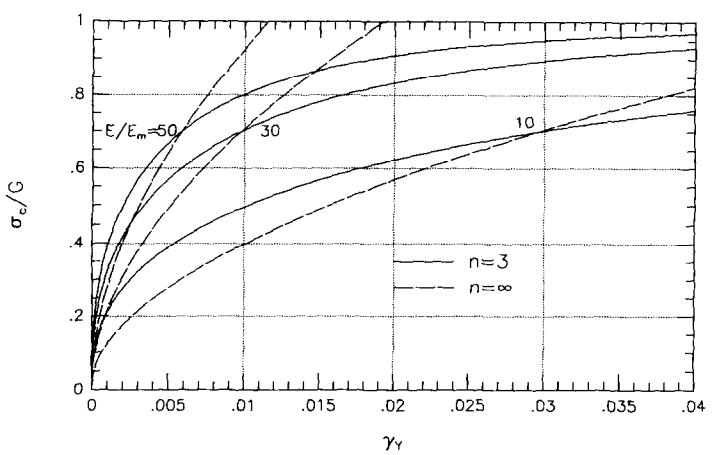

FIG. 11. Non-dimensional kinking stress ratio σ_c/G vs shear yield stress γ_Y of the composite; perfectly aligned, extensional fibres. Ramberg–Osgood hardening index = n; ratio of composite and matrix moduli = E/E_m.

It is interesting to note from (90) that for any given value of E/E_m, the curves of σ_c/G vs γ_Y for all values of n intersect at the value $\sigma_c/G = 0.7$. Thus, for $E/E_m = 30$, $\sigma_c/G = 0.7$ at $\gamma_Y = 0.0098$ at each n. Above this critical value of γ_Y, σ_c/G is an increasing function of n, and below it decreases with n.

The main conclusion we draw from the curves is that for realistic values of γ_Y in the vicinity of 0.01, the reduction of σ_c/G from the Rosen value of unity is quite insufficient to account for most of the experimental data in Fig. 2. The typically observed experimental knockdown factors of around 1/4 are predicted by (90) only for unrealistically low values of γ_Y and E/E_m. This further strengthens the case for the necessity of invoking initial misalignments to account for observed kinking stresses.

It remains reasonable to inquire about the plasticity effect of finite fibre stiffness on the kinking stress when initial imperfections *are* present. We study this question in the next section.

Initially misaligned fibres

If the fibres are presumed to have an initial rotation $\bar{\phi}$ in a narrow, $\beta = 0$ kink band, application of the remote stress σ^∞ will induce a state of combined axial compression and shear (σ_m, τ_m) in the matrix, and the J_2-deformation theory relations may be written as

$$\varepsilon_m = \frac{\sigma_m}{E_{ms}(\sigma_{me})}, \tag{91}$$

$$\gamma_m = \left[\frac{1}{G_m} + \frac{3}{E_{ms}(\sigma_{me})} - \frac{3}{E_m}\right]\tau_m \equiv \frac{\tau_m}{\bar{G}_m}, \tag{92}$$

where E_{ms} is now a function of the effective stress σ_{me} given by (82). (We are presuming a state of plane stress in the kink band, whereas it would be more appropriate to impose the condition that transverse strains in the narrow kink are constrained to equal those produced by σ^∞ in the unkinked regions; but this minor simplification is unlikely to affect our conclusions very much.) Following the calculations of the previous section, we rewrite the connection (78) between σ^∞ and σ_m as

$$\frac{\sigma^\infty}{G} = \sqrt{3}\gamma_Y\left[\frac{E}{E_m} + \left(\frac{E}{E_m} - 1 + v_f\right)\left(\frac{E_m}{E_{ms}(\sigma_{me})} - 1\right)\right]\frac{\sigma_m}{\sigma_{mY}} \tag{93}$$

and the use of (92) and the approximations (85) in the equilibrium equation (45) gives

$$\frac{\sigma^\infty}{G} = \frac{\tau/\tau_Y}{(\tau/\tau_Y)(G_m/\bar{G}_m) + \bar{\phi}/\gamma_Y}. \tag{94}$$

Rewriting (82) for σ_{me} in the form

$$\left(\frac{\sigma_{me}}{\sigma_{mY}}\right)^2 = \left(\frac{\sigma_m}{\sigma_{mY}}\right)^2 + \left(\frac{\tau}{\tau_Y}\right)^2 \tag{95}$$

and using (93)–(94) to eliminate σ_m/σ_{mY} and τ/τ_Y gives

$$\left(\frac{\sigma_{me}}{\sigma_{mY}}\right)^2 = \frac{\left(\frac{\sigma^\infty}{G}\right)^2\left(\frac{\bar{\phi}}{\gamma_Y}\right)^2}{\left[1-\left(\frac{\sigma^\infty}{G}\right)\left(\frac{G_m}{\bar{G}_m}\right)\right]^2} + \frac{\left(\frac{\sigma^\infty}{G}\right)^2}{3\gamma_Y^2\left[\frac{E}{E_m}+\left(\frac{E}{E_m}-1+v_f\right)\left(\frac{E_m}{E_{ms}}-1\right)\right]^2}. \tag{96}$$

Note that the defining relation (92) for $\bar{G}_m$ together with the Ramberg–Osgood formulas imply

$$\frac{G_m}{\bar{G}_m} - 1 = \rho\left(\frac{E_m}{E_{ms}} - 1\right) = b\left(\frac{\sigma_{me}}{\sigma_{mY}}\right)^{n-1}, \tag{97}$$

where ρ is defined by (75), and so (96) relates σ^∞/G to σ_{me}/σ_{mY}. For increasing values of σ_{me}/σ_{mY}, we can solve (96) numerically for σ^∞/G, and so find the non-dimensional kinking stress σ_c/G when σ^∞/G reaches a maximum. Numerical results for σ_c/G vs $\bar{\phi}/\gamma_Y$ are shown in Fig. 12 for $n = 3$ and several values of γ_Y that cover the practical

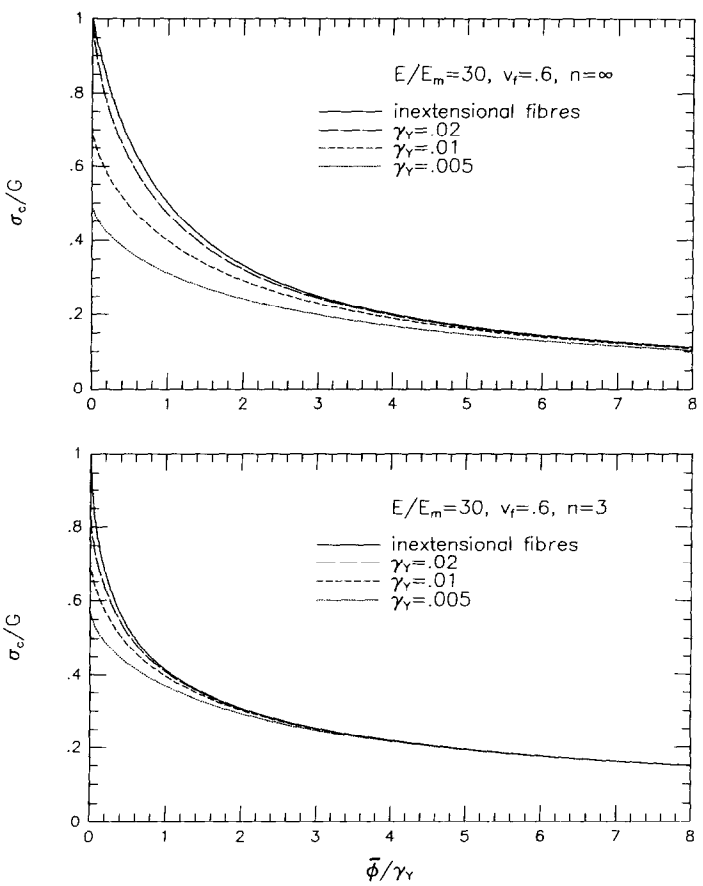

FIG. 12. Non-dimensional kinking stress ratio σ_c/G vs fibre imperfection ratio $\bar{\phi}/\gamma_Y$; extensional fibres.

range; the inextensional-fibre result of Fig. 4 is shown for comparison. The parameters $E/E_m = 30$ and $v_f = 0.6$ were used, and it is striking that for these values, typical for polymer matrices, plasticity effects on σ_c of finite fibre stiffness become negligible for $\bar{\phi}/\gamma_Y > 2$.

The analogous set of curves for $n = \infty$ shown in the top part of Fig. 12 show that for high values of n, larger, but still quite small, effects of finite fibre stiffness might occur at moderate values of $\bar{\phi}/\gamma_Y$. {The calculation of these results for $n = \infty$ required a special set-up. Under increasing σ^∞/G the composite responds elastically until the yield condition $\sigma_{me}/\sigma_{mY} = 1$ is satisfied. From (96) this implies that

$$\frac{\left(\frac{\sigma^\infty}{G}\right)^2\left(\frac{\bar{\phi}}{\gamma_Y}\right)^2}{\left[1-\left(\frac{\sigma^\infty}{G}\right)\right]^2} + \frac{\left(\frac{\sigma^\infty}{G}\right)^2}{3\gamma_Y^2\left[\frac{E}{E_m}\right]^2} = 1 \tag{98}$$

at yield. Thereafter, we can track the evolution of σ^∞/G by using

$$1 = \frac{\left(\frac{\sigma^\infty}{G}\right)^2\left(\frac{\bar{\phi}}{\gamma_Y}\right)^2}{\left[1-\left(\frac{\sigma^\infty}{G}\right)\left(\frac{G_m}{\bar{G}_m}\right)\right]^2} + \frac{\left(\frac{\sigma^\infty}{G}\right)^2}{3\gamma_Y^2\left[\frac{E}{E_m}+\frac{1}{\rho}\left(\frac{E}{E_m}-1+v_f\right)\left(\frac{G_m}{\bar{G}_m}-1\right)\right]^2} \tag{99}$$

to solve for σ^∞/G as $G_m/\bar{G}_m$ is increased from unity, as the independent variable. The maximum value of σ^∞/G can occur either at or beyond yield.}

We conclude that when realistic imperfections are present, and the longitudinal stiffness of the composite is large (>20) compared to the elastic matrix stiffness, and the yield strain of the composite is not unusually low (<0.005), then the assumption of axially rigid fibres is well justified.

Concluding Discussion

The theoretical and experimental evidence presented in this paper shows that long fibre polymeric composites, such as carbon fibre in an epoxy matrix or glass fibre in a polyester matrix, tend to fail in compression by plastic kinking. These kinking strengths are sensitive to the initial misalignment of the fibres, and show considerable scatter. For misaligned fibres, kinking stresses in the vicinity of 25% of the elastic microbuckling stresses of composites having perfectly straight, aligned fibres are typical. The basic analyses and quantitative results presented in this paper, encompassing effects of strain-hardening, kink inclination, and applied shear stress, provide a broad basis for the understanding of the kinking phenomenon. The analysis given of the effects of finite fibre stiffness provide theoretical justification for the assumption of rigid fibres in the study of many aspects of the kinking problem. However, the present treatment of kinking is unable to predict the width of the kink band and its

inclination; in order to make these predictions, a study of the initiation and growth of kinking patterns, with explicit inclusion of fibre bending resistance, is required.

A paucity of experimental data remains on the compressive failure of long-fibre ceramic-matrix and metal-matrix composites. In such composites the fibre-matrix stiffness ratios are substantially lower than those for polymer matrices. It is therefore clear from the trends established concerning the effects of finite fibre stiffness that the rigid-fibre assumption in the theoretical study of kinking in ceramic and metal matrix composites might not be justified. The importance of kinking as a failure mode in such composites has not been established.

ACKNOWLEDGEMENTS

This work was supported in part by the National Science Foundation under a Material Research Laboratory grant (DMR-89-20490), in part by a DARPA University Research Initiative grant (Subagreement P.O. No. VB38639-0 with the University of California, Santa Barbara, ONR Prime Contract 00014-86-K-0753), and by the Division of Applied Sciences, Harvard University. The authors are also grateful for funding from the Procurement Executive of the Ministry of Defence, under a joint SERC/MOD contract, and for support from the ONR contract 00014-91-J-1916.

REFERENCES

ARGON, A. S. 1972 In *Treatise of Materials Science and Technology*, Vol. 1. Academic Press, New York.

BARKER, A. J. and BALASUNDARAM, V. 1987 *Composites* **18**(3), 217.

BATDORF, S. B. and KO, R. W. C. 1987 Internal report, School of Engineering and Applied Science, University of California, Los Angeles, CA 90024.

BUDIANSKY, B. 1959 *J. Appl. Mech.* **26,** 259.

BUDIANSKY, B. 1979 In Preliminary Reports, Memoranda and Technical Notes of the Materials Research Council Summer Conference, La Jolla, CA, July 1979, Sponsored by DARPA.

BUDIANSKY, B. 1983 *Comp. Struct.* **16**(1), 3.

CHAPLIN, C. R. 1977 *J. Mater. Sci.* **12,** 347.

CHATTERJEE, S. N. and MCLAUGHLIN, P. V. 1979 *Proc. 3rd Engineering Mechanics Div. Specialty Conf.*, 17–19 Sept., 1979, University of Texas at Austin, pp. 649–652. ASCE, New York.

CURTIS, P. T. 1986 RAE Tech. Report 86021.

EVANS, A. G. and ADLER, W. F. 1978 *Acta Metall.* **26,** 725.

EWINS, P.D. and POTTER, R. T. 1980 *Phil. Trans. R. Soc. Lond.* **A294,** 507.

FLECK, N. A. and BUDIANSKY, B. 1991 *Proc. IUTAM Symp. on Inelastic Deformation of Composite Materials*, Troy, New York, 29 May–1 June, 1990 (edited J. DVORAK), pp. 235–273. Springer-Verlag, New York.

FRIED, N. 1963 *Proc. 18th Annual Meeting of the Reinforced Plastics Division, Society of Plastics Industry*, Section 9-A, pp. 1–10.

FRIED, N. and KAMINETSKY, J. 1964 *Proc. 19th Annual Meeting of the Reinforced Plastics Division, Society of Plastics Industry*, Section 9-A, pp. 1–10.

GIBSON, L. J. and ASHBY, M. F. 1988 *Cellular Solids: Structure and Properties*. Pergamon Press, Oxford.

GRESZCZUK, L. B. 1972 AFML-TR-72107, U.S. Air Force.

GRESZCZUK, L. B. 1975 *AIAA Jl.* **13**(10), 1311.

HAHN, H. T., SOHI, M. and MOON, S. 1986 NASA CR 3988.

HILL, R. 1979 *Math. Proc. Camb. Phil. Soc.* **55,** 179.

JELF, P. M. and FLECK, N. A. 1991 Submitted to *J. Comp. Mater.*

JELF, P. M., SOUTIS, C. and FLECK, N. A. 1990 Presented at 3rd. International Symposium on Composites, Patras, Greece, Sept. 1990.

JOHNSTON, N. J. and HERGENROTHER, P. M. 1987 *32nd Int. SAMPE Symposium*, 6–9 April 1987.

LAGER, J. B. and JUNE, R. R. 1969 *J. Comp. Mater.* **3**(1), 48.

LANKFORD, J. 1989 *Mat. Sci. Engng.* **A107,** 261.

MONCUNILL DE FERRAN, E. and HARRIS, B. 1970 *J. Comp. Mater.* **4,** 62.

PARRY, T. V. and WRONSKI, A. S. 1981 *J. Mat. Sci.* **16,** 439.

PETERS, R. W., DOW, N. F. and BATDORF, S. B. 1950 *Proc. Soc. Exp. Stress Analysis* **7,** 27.

PIGGOTT, M. R. 1981 *J. Mat. Sci.* **16,** 2837.

PIGGOTT, M. R. and HARRIS, B. 1980 *J. Mat. Sci.* **15,** 2523.

PIGGOTT, M. R. and WILDE, P. 1980 *J. Mat. Sci.* **15,** 2811.

PRANDY, J. M. and HAHN, H. T. 1990 *Proc. 35th International SAMPE Symposium*, 2–5 April 1990, pp. 1657–1670.

PURSLOW, D. 1986 RAE Technical Report 86046.

RHODES, M. D., MIKULAS, M. M. and MCGOWAN, P. E. 1984 *AIAA Jl* **22**(9), 1283.

ROSEN, B. W. 1965 *Fibre Composite Materials, Am. Soc. Metals Seminar*, Chapter 3. Am. Soc. Metals.

ROSEN, B. W. 1989 *Proc. 1st US/USSR Symposium on Mechanics of Composite Materials*, Riga, Latvia, May 1989. To be published by ASME.

SOUTIS, C., FLECK, N. A. and SMITH, P. A. 1991 *J. Compos. Mater.* **25,** 1476.

STARNES, J. H. and WILLIAMS, J. G. 1982 *Mechanics of Composites Materials–Recent Advances* (Edited by Z. HASHIN and C. T. HERAKOVICH), pp. 283–306. Pergamon Press, Oxford.

U.S. POLYMERIC 1990 Data sheets on properties of carbon fibre epoxy composites, 700E Dyer Rd., Santa Ana, CA, 92707, USA.

WARD, I. M. 1983 *The Mechanical Properties of Solid Polymers*, 2nd edn. Wiley, New York.

WILKINSON, E., PARRY, T. V. and WRONSKI, A. S. 1986 *Comp. Sci. Technol.* **26,** 17.

YOUNG, R. J. and YOUNG, R. 1990 *Proc. 4th European Conference on Composite Materials*, 25–28 September, Stuttgart, pp. 685–690. Elsevier Applied Science, Amsterdam.

YURGARTIS, S. W. 1987 *Comp. Sci. Technol.* **30,** 279.